Calculation of λ Modes of the Multi-group Neutron Transport Equation Using the Discrete Ordinates and Finite Difference Method

S. Morató[a], Á. Bernal[a], R. Miró[a], Jose E. Roman[b], G. Verdú[a,*]

[a] *Institute for Industrial, Radiophysical and Environmental Safety (ISIRYM) at the Universitat Politècnica de València, Spain*
[b] *Department of Information Systems and Computations (DSIC) at the Universitat Politècnica de València, Spain*

Abstract

The method explained in this paper solves the steady-state of the neutron transport equation for 1D and 2D systems modeled with Cartesian geometry, by using the Discrete Ordinates method S_N for the angular discretization and the finite difference method for the spatial discretization. The method applies the multi-group approach for any energy discretization, including upscattering terms. The method solves the steady-state equation by solving a generalized eigenvalue problem by means of a Krylov-Schur method. One of the main advantages of the method is the capability to calculate multiple eigenfunctions. The Discrete Ordinates methodology is used for the angular discretization, which uses a simple formulation involving the angles and direction cosines. The spatial discretization with finite difference method is selected for its simplicity. The method is validated with several one-dimensional benchmark problems and four two dimensional benchmark problems. The results show good agreement with respect to the reference results for all the cases studied.

Keywords: Neutron transport, Discrete ordinates, Multigroup, Finite Difference Method, Multiple Eigenvalues, Anisotropic

1. Introduction

The power generated inside nuclear reactors is one of the most important parameters in Nuclear Safety Analyses. The energy is released by the nuclear fissions inside the reactor core, which is proportional to the neutron flux. Therefore, the calculation of the neutron flux distribution can determine the spatial and time distribution of the power.

*Corresponding author
Email address: gverdu@iqn.upv.es (G. Verdú)

Then, the analysis and design of nuclear reactors are based on the neutron distribution in the system and the most accurate manner of calculating the neutron population is by solving the Neutron Transport Equation. This equation depends on the spatial variables, neutron energy, angular direction and time [1]. Although, the real number of neutrons per unit volume is continuously varying with time, even steady-state conditions, under this assumption, the number density of neutrons oscillates about an average value related to the solution of the steady state of the neutron transport equation. Many fields of nuclear engineering make use of a solution of the transport equation, such as, reactor physics, in Nuclear Safety and Criticality, and in radiation shielding and protection.

The spatial distribution of the neutron flux can be determined by solving the steady state of the neutron transport equation. Analytical solutions are available in very limited cases, thus, it is necessary to apply numerical methods and discretize some variables. The variables to be discretized are the neutron energy, angular direction and spatial variables.

The multi-energy-group approximation is commonly used for the energy discretization. So, the neutron transport equation can be written in multi-group form, leading to a set of *G-coupled* (G is the total number of groups) integro-differential equations.

For the angular discretization there are two commonly used methods : Discrete Ordinates (S_N) and Spherical Harmonics (P_N). The method selected in this work is discrete ordinates, in which the angular variable is discretized into a set of directions. Then, the transport equation is written for each direction, including coupling terms that describe direction to direction transfer. This is the most popular and easiest method in numerical transport calculation. However, the major disadvantage of the S_n method is the well-known *ray effect* [2]. One simple solution for this problem could be to introduce additional discrete directions, although this does not always work. Another proposed solution is to transform the discrete ordinates equations to spherical-harmonics like form. On the other hand, spherical harmonics method is based on a truncated polynomial expansion in spherical harmonics of the flux. This method might be more accurate but it is meaningfully more complex than S_n method.

There are several spatial discretization methods. They are generally classified into three groups: Finite Difference Methods (FDM), Finite Volume Methods (FVM) and Finite Element Methods (FEM). Due to the simplicity of the method when Cartesian meshes are used, FDM has been selected for this work. However FDM may present some disadvantages. First, FDM is generally not conservative because it approximates the neutron flux at grid points. Second, the obtained matrices might present singularities.

The discretized steady-state neutron transport equation [3, 4] can be transformed into a generalized eigenvalue problem. Although most methods usually calculate the largest eigenvalue, the calculation of several eigenvalues and eigenvectors can be important for different applications such as the modal analysis of nuclear reactors and BWR instabilities analysis or flux fluctuations in certain PWR. One goal of this work is to develop a methodology for calculating

multiple eigenvalues of the multi-group neutron transport equation.

Nevertheless, the solution of the generalized eigenvalue problem could not be an easy task due to the large and sparse nature of the obtained matrices. This work solves the eigenvalue problem by means of the Krylov-Schur algorithm implemented in the SLEPc library, and calculating several modes. SLEPc is the Scalable Library for Eigenvalue Problem Computations, a software library for the solution of large, sparse eigenproblems on parallel computers [5].

SLEPc is the state of art for calculating eigenproblems of large and sparse matrices like those obtained with the method of this paper. In addition, SLEPc uses PETSc [6] (Portable, Extensible Toolkit for Scientific Computation) to extend it with all the functionality necessary for the solution of eigenvalue problmes, which includes matrix operations and solution of linear systems.

Discrete ordinates method S_N is commonly used in several codes such as $DORT/TORT$ (Rhoades and Childs, 1993) [7], $DANTSYS$ (Alcouffe et al., 1995) [8],$PARTISN$ (Alcouffe eta al., 2005) [9], $PENTRAN$ (Sjoden and Haghighat, 1996) [10] and $DRAGON$ (Marleau et al., 2008) [11]. Other authors use different methods, such as Spherical Harmonics (P_N), simplified P_N (SP_N), Method of Characteristics (MOC). MOC method has been implemented in some current research codes like $MPact$ code from the University of Michigan [12], the $nTRACER$ code from Seoul National University [13] and $DRAGON$ code from Êcole Polytechnique de Montréal. On the other hand, one of the most accurate methods is NCM applied in (Capilla et. al) [14] to neutron transport problems calculating also multiple eigenvalues. Most of the aforementioned S_N codes only calulate the first eigenvalue.

Then, this work develops a methodology to solves the Neutron Transport Equation with S_N, FDM and calculating several eigenvalues and eigenvectors by means of Krylov Schur of SLEPc. Several angular quadratures for the S_N method were implemented, such as, Level-Symmetric, Gauss-Legendre, and Legendre-Chebyshev [15, 16]. This paper shows a simple formulation for the equations, including any kind of up-scattering. Also, a boundary conditions analysis is carry out for different boundary conditions.

The outline of the paper is as follows. Section 2 explains the discretization of the equations and the methodology used. Section 3 describes the benchmarks used to validate the method and their results. Section 4 contains few comments and conclusions about the results.

2. Methods

2.1. One-dimensional case

The one-dimensional steady-state Neutron Transport Equation [17] can be expressed as in Eq. 1 :

$$\mu\frac{\partial\psi(x,\mu,E)}{\partial x}+\Sigma_t(x,E)\psi(x,\mu,E)=\int_0^\infty\int_{-1}^1\Sigma_s(x,\mu',\mu,E'\to E)\psi(x,\mu',E')d\mu'dE' + \frac{1}{K_{eff}}\chi(x,E)\int_0^\infty\int_{-1}^1\nu(x,E')\Sigma_f(x,E')\psi(x,\mu',E')d\mu'dE' \tag{1}$$

Where:

x : Spatial variable
μ : Angular variable or director cosine
E : Energy
$\psi(x,\mu,E)$: Angular neutron flux
$\Sigma_t(x,E)$: Macroscopic total cross-section
$\Sigma_s(x,\mu',\mu,E'\to E)$: Macroscopic scattering cross-section from energy E' to E and from direction μ' to μ
$\chi(x,E)$: Fission spectrum
$\nu(x,E')$: Average number of neutrons generated per fission
$\Sigma_f(x,E')$: Macroscopic fission cross-section
K_{eff} : Multiplication Factor

To derive multi-group equations, one first divide the neutron energy range into G intervals. The particles in group g are taken to be just those with energies between E_g and E_{g-1}, hence the group number increases as the energy decreases. Then the angular flux for group g can be expressed as:

$$\psi_g(x,\mu)=\int_{E_g}^{E_{g-1}}\psi(x,\mu,E)dE \tag{2}$$

And if one proceed by dividing the energy integrals in Eq. 1, into the contributions for each energy group:

$$\int_0^\infty\psi(x,\mu,E')dE'=\sum_{g'=1}^{G}\int_{E_{g'}}^{E_{g'-1}}\psi(x,\mu,E')dE' \tag{3}$$

For brevity the shorthand notation of the Eq. 4 is employed:

$$\int_g dE=\int_{E_g}^{E_{g-1}}dE \tag{4}$$

and integrating between E_g and E_{g-1} one obtain:

$$\mu\frac{\partial}{\partial x}\int_g \psi(x,\mu,E)dE + \int_g \Sigma_t(x,E)\psi(x,\mu,E)dE$$
$$= \sum_{g'=1}^{G}\int_g\int_{g'}\int_{-1}^{1}\Sigma_s(x,\mu',\mu,E'\to E)\psi(x,\mu',E')d\mu'dE'dE$$
$$+\frac{1}{K_{eff}}\int_g \chi(x,E)\sum_{g'=1}^{G}\int_{g'}\int_{-1}^{1}\nu(x,E')\Sigma_f(x,E')\psi(x,\mu',E')d\mu'dE'dE \tag{5}$$

Assuming that within each energy group the angular flux can be approximated as the product of a known function of energy $f(E)$ and the group flux $\psi_g(x,\mu)$, the multigroup cross sections can be defined as:

$$\Sigma_{t,g}(x) = \int_g \Sigma_t(x,E)f(E)dE \tag{6}$$

$$\nu(x)\Sigma_{f,g}(x) = \int_g \nu(x,E)\Sigma_f(x,E)f(E)dE \tag{7}$$

$$\Sigma_{s,g'\to g}(x,\mu',\mu) = \int_g\int_{g'}\Sigma_s(x,\mu',\mu,E'\to E)f(E')dE'dE \tag{8}$$

and let:

$$\chi_g(x) = \int_g \chi(x,E)dE \tag{9}$$

and considering:

$$\int_g f(E)dE = 1 \tag{10}$$

then one may write Eq. 5 in the conventional multi-group form:

$$\mu\frac{\partial}{\partial x}\psi_g(x,\mu) + \Sigma_{t,g}(x)\psi_g(x,\mu)$$
$$= \sum_{g'=1}^{G}\int_{-1}^{1}\Sigma_{s,g'\to g}(x,\mu',\mu)\psi_{g'}(x,\mu')d\mu'$$
$$+\frac{1}{K_{eff}}\chi_g(x)\sum_{g'=1}^{G}\int_{-1}^{1}\nu_{g'}(x)\Sigma_{f,g'}(x)\psi_{g'}(x,\mu')d\mu' \tag{11}$$

On the other hand, the anisotropic scattering cross section is commonly written as a Legendre Polynomial Expansion and the angular flux can be expanded as a Legendre series of degree L. [17].

$$\int_{-1}^{1} \Sigma_{s,g'\to g}(x,\mu',\mu)\psi_g(x,\mu')d\mu' = \int_{-1}^{1} \sum_{k=0}^{\infty}(2k+1)\Sigma_{s,g'\to g,k}(x)P_k(\mu)P_k(\mu')\sum_{l=0}^{L}(2l+1)P_l(\mu')\phi_{g',l}(x)d\mu' \tag{12}$$

Considering the orthogonality relation of the Legendre Polynomials:

$$\int_{-1}^{1} P_k(\mu)P_l(\mu)d\mu = \frac{1}{2l+1}\delta_{kl} \tag{13}$$

with δ_{kl} *Kronecker* delta, equal to 1 if $k = l$ and 0 otherwise. The Eq. 12 takes the form:

$$\int_{-1}^{1} \Sigma_{s,g'\to g}(x,\mu',\mu)\psi_g(x,\mu')d\mu' = \sum_{l=0}^{L} P_l(\mu)\Sigma_{s,g'\to g,l}(x)\phi_{g',l}(x) \tag{14}$$

The Legendre moments $\Sigma_{s,g'\to g,l}$ are typically calculated and stored for each material region [4]. The Discrete Ordinates method consists in considering only a set of directions μ_n and apply a quadrature approximation to the integral term. To solve the equation, one can define N discrete directions $(\mu_1, \mu_2, ..., \mu_N)$ with $-1 \leq \mu \leq +1$ and corresponding weighting coefficients $(w_1, w_2, ..., w_N)$. In Discrete Ordinates equations the scalar flux is approximated by the following quadrature formula:

$$\phi(x) = \int_{-1}^{1} \psi(x,\mu)d\mu = \frac{1}{2}\sum_{n=1}^{N} w_n\psi(x,\mu_n) \tag{15}$$

and the Legendre moments by:

$$\phi_l(x) = \frac{1}{2}\sum_{n=1}^{N} w_n P_l(\mu_n)\psi(x,\mu_n) \tag{16}$$

Note that both the flux and the Legendre moment approximation are divided by 2, that is because the quadrature formula is normalized by

$$\sum_{n=1}^{N} w_n = 2 \quad \text{with} \quad w_n > 0 \tag{17}$$

Including Eqs. 14-16 into Eq. 11, it is reformulated as:

$$\mu\frac{\partial\psi_g(x,\mu)}{\partial x} + \Sigma_{t,g}(x)\psi_g(x,\mu) = \sum_{g'=1}^{G}\sum_{l=0}^{L} P_l(\mu)\Sigma_{s,g'\to g,l}(x)\frac{1}{2}\sum_{n=1}^{N} w_n P_l(\mu_n)\psi_{g'}(x,\mu_n) + \frac{1}{K_{eff}}\chi_g(x)\sum_{g'=1}^{G}\nu_{g'}(x)\Sigma_{f,g'}(x)\frac{1}{2}\sum_{n=1}^{N} w_n\psi(x,\mu_n) \quad (18)$$

The choice of the weighting factors w_N is commonly made with respect to an even number of discrete ordinates μ_N chosen in a symmetric way with respect to $\mu = 0$. Hence, one can define this group of directions and corresponding weighting coefficients as:

$$\mu_n > 0$$
$$\mu_{N+1-n} = -\mu_n \quad \text{for} \quad n = 1, 2, ..., \frac{N}{2}.$$
$$w_{N+1-n} = w_n \quad (19)$$

Finally, the Finite Difference Method for the spatial discretization is used. To discretize the spatial variable one define a one-dimensional spatial grid with I mesh points. The cross-sections are taken to be constant inside each interval $(x_{i-1/2}, x_{i+1/2})$. Moreover, the cell-centered points are defined by:

$$x_i = \frac{1}{2}(x_{i-1/2} + x_{i+1/2}) \quad (20)$$

and defining:

$$\Sigma(x) = \Sigma(i) \quad \text{with} \quad x_{i-1/2} < x < x_{i+1/2} \quad (21)$$

The flux derivative term and the flux are approximated by:

$$\frac{\partial}{\partial x}\psi_g(x,\mu) = \frac{\psi_g(i+1/2,\mu_n) - \psi_g(i-1/2,\mu_n)}{h} \quad (22)$$

$$\psi_g(x,\mu) = \frac{\psi_g(i+1/2,\mu_n) + \psi_g(i-1/2,\mu_n)}{2} \quad (23)$$

where $h = x_{i+1/2} - x_{i-1/2} = \Delta x_i$.

Then, the Eq. 18 is converted into multi-group steady-state Neutron Transport Equation with S_N and FDM discretizations:

$$\mu_n \frac{\psi_g(i+1/2,\mu_n)-\psi_g(i-1/2,\mu_n)}{h}+\Sigma_{t,g}(i)\frac{\psi_g(i+1/2,\mu_n)+\psi_g(i-1/2,\mu_n)}{2}$$
$$-\frac{1}{4}\sum_{g'=1}^{G}\sum_{l=0}^{L}\Sigma_{s,g'\to g,l}(i)P_l(\mu_n)\sum_{m=1}^{N}w_m[\psi_{g'}(i+1/2,\mu_m)+\psi_{g'}(i-1/2,\mu_m)]P_l(\mu_m)$$
$$=\frac{1}{K_{eff}}\frac{\chi_g(i)}{4}\sum_{g'=1}^{G}\nu_{g'}\Sigma_{f,g'}(i)\sum_{m=1}^{N}w_m[\psi_{g'}(i+1/2,\mu_m)+\psi_g(i-1/2,\mu_m)] \tag{24}$$

Where:

$1 \le n \le N$ with N the number of discrete directions
$1 \le g \le G$ with G the total number of energy groups
$0 \le l \le L$ with L the order of the *Legendre* polynomial scattering expansion
w_m are the weighting coefficients of directions μ_m and i is the mesh cell number

2.2. Two-dimensional case

The two-dimensional steady-state Neutron Transport Equation can be expressed as:

$$\mu\frac{\partial\psi(x,y,\hat{\Omega},E)}{\partial x}+\eta\frac{\partial\psi(x,y,\hat{\Omega},E)}{\partial y}+\Sigma_t(x,y,E)\psi(x,y,\hat{\Omega},E)=$$
$$\int_0^\infty\int_{4\pi}\Sigma_s(x,y,\hat{\Omega}'\to\hat{\Omega},E'\to E)\psi(x,y,\hat{\Omega}',E')d\hat{\Omega}'dE'$$
$$+\frac{1}{K_{eff}}\frac{\chi(x,y,E)}{4\pi}\int_0^\infty\int_{4\pi}\nu(x,y,E')\Sigma_f(x,y,E')\psi(x,y,\hat{\Omega}',E')d\hat{\Omega}'dE' \tag{25}$$

Where

$$
\begin{aligned}
x, y &: \text{Spatial variables} \\
\theta &: \text{Polar angle} \\
\varphi &: \text{Azimuthal angle} \\
\hat{\Omega} &: = \mu \overrightarrow{i} + \eta \overrightarrow{j} + \xi \overrightarrow{k} \\
\mu &: cos(\theta) \\
\eta &: \sqrt{(1-\mu^2)} cos(\varphi) \\
\xi &: \sqrt{1-\mu^2-\eta^2} \\
E &: \text{Energy} \\
\psi(x, y, \hat{\Omega}, E) &: \text{Angular neutron flux} \\
\Sigma_t(x, y, E) &: \text{Macroscopic total cross-section} \\
\Sigma_s(x, y, \hat{\Omega}' \to \hat{\Omega}, E' \to E) &: \text{Macroscopic scattering cross-section} \\
&\quad \text{from energy } E' \text{ to } E \text{ and from direction } \hat{\Omega}' \text{ to } \hat{\Omega} \\
\chi(x, y, E) &: \text{Fission spectrum} \\
\nu(x, y, E') &: \text{Average number of neutrons generated per fission} \\
\Sigma_f(x, y, E') &: \text{Macroscopic fission cross-section}
\end{aligned}
$$

Similarly to one-dimensional case, the multi-group equation takes the form:

$$
\begin{aligned}
\mu \frac{\partial}{\partial x} \int_g \psi(x, y, \hat{\Omega}, E) dE + \eta \frac{\partial}{\partial y} \int_g \psi(x, y, \hat{\Omega}, E) dE + \int_g \Sigma_t(x, y, E) \psi(x, y, \hat{\Omega}, E) dE = \\
\sum_{g'=1}^{G} \int_g \int_{g'} \int_{4\pi} \Sigma_s(x, y, \hat{\Omega}' \to \hat{\Omega}, E' \to E) \psi(x, y, \hat{\Omega}', E') d\hat{\Omega}' dE' dE \\
+ \frac{1}{K_{eff}} \frac{\chi(x, y, E)}{4\pi} \sum_{g'=1}^{G} \int_{g'} \int_{4\pi} \nu(x, y, E') \Sigma_f(x, y, E') \psi(x, y, \hat{\Omega}', E') d\hat{\Omega}' dE' dE
\end{aligned}
\tag{26}
$$

And introducing the multi-group cross-sections like in the Equations 6,7 and 8:

$$\mu\frac{\partial}{\partial x}\psi_g(x,y,\hat{\Omega})+\eta\frac{\partial}{\partial y}\psi_g(x,y,\hat{\Omega})+\Sigma_{t,g}(x,y)\psi_g(x,y,\hat{\Omega})= \sum_{g'=1}^{G}\int_{4\pi}\Sigma_{s,g'\to g}(x,y,\hat{\Omega}'\to\hat{\Omega})\psi_{g'}(x,y,\hat{\Omega}')d\hat{\Omega}' + \frac{1}{K_{eff}}\frac{\chi_g(x,y)}{4\pi}\sum_{g'=1}^{G}\int_{4\pi}\nu_{g'}(x,y)\Sigma_{f,g'}(x,y)\psi_{g'}(x,y,\hat{\Omega}')d\hat{\Omega} \quad (27)$$

Similar to one-dimensional case the scalar flux can be approximated by quadrature formula:

$$\phi(x,y)=\int_0^{2\pi}\int_{-1}^{1}\psi(x,y,\mu,\varphi)d\mu d\varphi=\frac{1}{8}\sum_{n=1}^{N}w_n\psi(x,y,\mu_n,\varphi_n)=\frac{1}{8}\sum_{n=1}^{N}w_n\psi(x,y,\mu_n,\eta_n) \quad (28)$$

From here, the scattering term will be dealt with separately.

$$\mu_n\frac{\partial\psi_g(x,y,\mu_n,\eta_n)}{\partial x}+\eta_n\frac{\partial\psi_g(x,y,\mu_n,\eta_n)}{\partial y}+\Sigma_{t,g}(x,y,E)\psi_g(x,y,\mu_n,\eta_n)= q_s(x,y)+\frac{1}{K_{eff}}\frac{\chi_g(x,y)}{8}\sum_{g'=1}^{G}\nu_{g'}(x,y)\Sigma_{f,g'}(x,y)\sum_{m=1}^{N}w_m\psi_{g'}(x,y,\mu_m,\eta_m) \quad (29)$$

Where $q_s(x,y)$ term can be , like in the one-dimensional case, expanded with Legendre Polinomials , but in this case, it is also necessary to use an Spherical Harmonics Expansion for the angular flux defined in terms of the Associated Legendre Polynomials [17, 18]. Then the q_s term is expressed as:

$$q_s(x,y)=\frac{1}{8}\sum_{g'=1}^{G}\sum_{l=0}^{L}(2l+1)\Sigma_{s,g'\to g,l}(x,y)\{P_l(\mu_n)\sum_{m=1}^{N}w_mP_l(\mu_m)\psi_{g'}(x,y,\mu_m\eta_m) + 2\sum_{k=1}^{l}\frac{(l-k)!}{(l+k)!}P_l^k(\mu_n)[\sum_{m=1}^{N}w_mP_l^k(\mu_m)\psi_{g'}(x,y,\mu_m,\eta_m)cos(k\varphi_m)cos(k\varphi_n) + \sum_{m=1}^{N}w_mP_l^k(\mu_m)\psi_{g'}(x,y,\mu_m,\eta_m)sin(k\varphi_m)sin(k\varphi_n)]\} \quad (30)$$

Note that, both terms, scattering and fission, are divided by 8. This is because the weights corresponding to each octant are normalized to sum 1. Rearranging

terms:

$$q_s(x,y) \quad = \quad \frac{1}{8}\sum_{g'=1}^{G}\sum_{m=1}^{N} w_m \psi_{g'}(x,y,\mu_m,\eta_m) \quad \cdot \quad \Sigma_{s,g'\to g,L,n,m}(x,y) \quad (31)$$

Where

$$\Sigma_{s,g'\to g,L,n,m}(x,y) = \sum_{l=0}^{L}(2l+1)\Sigma_{s,g'\to g,l}(x,y)\{P_l(\mu_n)P_l(\mu_m) + 2\sum_{k=1}^{l}\frac{(l-k)!}{(l+k)!}P_l^k(\mu_n)P_l^k(\mu_m)[cos(k(\varphi_n-\varphi_m))]\} \quad (32)$$

To reduce the number of equations by half without loss of precision, the authors have decided to use the property of symmetry for the case of 2D plane geometry with respect to the polar angle. This can be demonstrated if one can consider
145 that $\mu_1 = \mu_2$ and $\varphi_1 = -\varphi_2$ due to the z-axis symmetry explained at Fig. 1

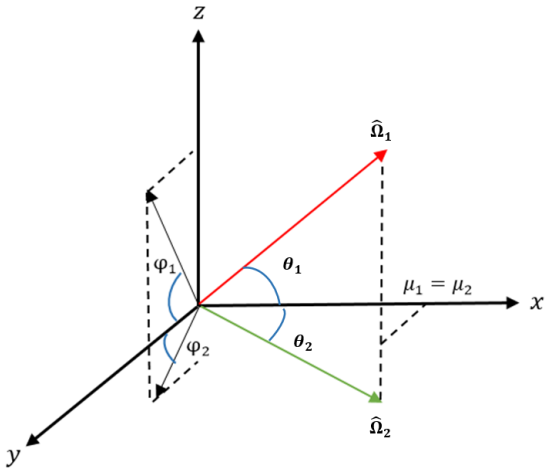

Figure 1: Symmetry

For the previous two directions, one can sum the terms $\Sigma_{s,g'\to g,L,n,m}$ as in Eq. 33:

$$\Sigma_{s,g'\to g,L,n,1}(x,y) + \Sigma_{s,g'\to g,L,n,2}(x,y)$$
$$= \sum_{l=0}^{L}(2l+1)\Sigma_{s,g'\to g,l}(x,y)\{P_l(\mu_n)[P_l(\mu_1) + [P_l(\mu_2)]$$
$$+ 2\sum_{k=1}^{l}\frac{(l-k)!}{(l+k)!}P_l^k(\mu_n)[P_l^k(\mu_1)[cos(k(\varphi_n-\varphi_1))] + P_l^k(\mu_2)[cos(k(\varphi_n-\varphi_2))]]\}$$
$$= \sum_{l=0}^{L}(2l+1)\Sigma_{s,g'\to g,l}(x,y)\{P_l(\mu_n)[2P_l(\mu_1)]$$
$$+ 2\sum_{k=1}^{l}\frac{(l-k)!}{(l+k)!}P_l(\mu_n)P_l^k(\mu_1)[cos(k(\varphi_n-\varphi_1))] + [cos(k(\varphi_n+\varphi_1))]\} \quad (33)$$

Using the trigonometry relation $cos(x \pm y) = cos(x)cos(y) \mp sin(x)sin(y)$ the Eq. 33 is simplified as scattering term considering the whole unit sphere (3D) [19]:

$$\Sigma_{s,g'\to g,L,n,m}(x,y)^{3D} = 2\sum_{l=0}^{L}(2l+1)\Sigma_{s,g'\to g,l}(x,y)\{P_l(\mu_n)[P_l(\mu_1)]$$
$$+ 2\sum_{k=1}^{l}\frac{(l-k)!}{(l+k)!}P_l^k(\mu_n)P_l^k(\mu_1)[cos(k\varphi_n)cos(k\varphi_1)]\} \quad (34)$$

and then if one want only consider a unit semi-sphere (2D):

$$\Sigma_{s,g'\to g,L,n,m}(x,y)^{2D} = \frac{\Sigma_{s,g'\to g,L,n,m}(x,y)^{3D}}{2} = \sum_{l=0}^{L}(2l+1)\Sigma_{s,g'\to g,l}(x,y)\{P_l(\mu_n)[P_l(\mu_m)]$$
$$+ 2\sum_{k=1}^{l}\frac{(l-k)!}{(l+k)!}P_l^k(\mu_n)P_l^k(\mu_m)[cos(k\varphi_n)cos(k\varphi_m)]\} \quad (35)$$

Note that for the new formulation changed the consideration of 8 octants to 4, since only the positive polar angles are considered. Then, the sum of weighting coefficients is 4 and the q_s term and fission term will be divided now by 4.

$$q_s^{2D}(x,y) = \frac{1}{4}\sum_{g'=1}^{G}\sum_{m=1}^{N} w_m\psi_{g'}(x,y,\mu_m,\eta_m) \cdot \Sigma_{s,g'\to g,L,n,m}(x,y)^{2D} \quad (36)$$

Therefore, Eq. 37 is the 2D version of the Eq. 29.

$$\mu_n \frac{\partial \psi_g(x,y,\mu_n,\eta_n)}{\partial x} + \eta_n \frac{\partial \psi_g(x,y,\mu_n,\eta_n)}{\partial y} + \Sigma_{t,g}(x,y,E)\psi_g(x,y,\mu_n,\eta_n) = q_s^{2D}(x,y) + \frac{1}{K_{eff}} \frac{\chi_g(x,y)}{4} \sum_{g'=1}^{G} \nu_{g'}(x,y)\Sigma_{f,g'}(x,y) \sum_{m=1}^{N} w_m \psi_{g'}(x,y,\mu_m,\eta_m) \tag{37}$$

With this formulation, the number of considered directions is the half than if the whole unit sphere is considered. Consequently, the number of equations is reduced by half.

The Finite Difference Method is used for calculating the spatial derivatives and the cell average value of the angular neutron flux, as shown in Eq. 38-40. In these equations, $\psi_{i,j}^n$ is the angular neutron flux for the direction n and the node i,j. Fig. 2 shows an example of the numbering of the nodes.

$$\frac{\partial \psi_g(x,y,\mu_n,\eta_n)}{\partial x} = \frac{\psi_{i,j}^n + \psi_{i,j-1}^n - \psi_{i-1,j}^n - \psi_{i-1,j-1}^n}{2h} \tag{38}$$

$$\frac{\partial \psi_g(x,y,\mu_n,\eta_n)}{\partial y} = \frac{\psi_{i,j}^n + \psi_{i-1,j}^n - \psi_{i,j-1}^n - \psi_{i-1,j-1}^n}{2k} \tag{39}$$

$$\psi_g(x,y,\mu_n,\eta_n) = \frac{\psi_{i,j}^n + \psi_{i-1,j}^n + \psi_{i,j-1}^n + \psi_{i-1,j-1}^n}{4} \tag{40}$$

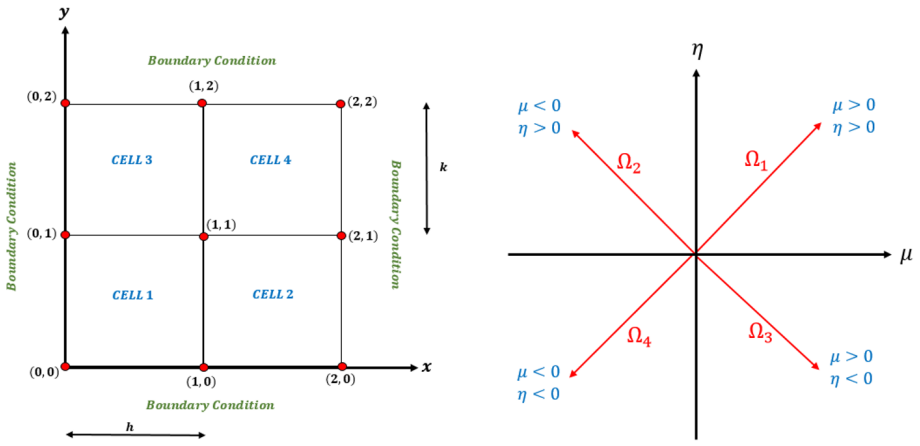

Figure 2: Spatial discretization and 2D angular distribution example for S_2

2.3. Boundary Conditions

The boundary conditions commonly used in neutron transport problems are vacuum, periodic, reflective and albedo conditions. One of the advantages of considering an even ordinate set for one-dimensional cases is that the vacuum, reflective or albedo boundary conditions are simply approximated by

$$\begin{aligned} \psi_n(i) = \beta \cdot \psi_{N+1-n}(i) \qquad \text{with} \quad & i = 0 \quad \text{and} \quad n = 1, 2, ..., N/2 \\ & \textit{or} \\ & i = I \quad \text{and} \quad n = \frac{N}{2} + 1, \frac{N}{2} + 2, ..., N \end{aligned} \tag{41}$$

where if

$\beta = 0$ (vacuum condition) ; $\beta = 1$ (reflective condition) ; $\beta \in$ (0 , 1) (albedo condition)

Vacuum, reflective and albedo condition can be expressed similarly to one-dimensional case using Eq. 42 for two-dimensional cases, in which the only difference is the β value.

$$\begin{aligned} \psi^n_{i,j} &= \beta \cdot \psi^{\frac{N}{2}+1-n}_{0,j} \; ; 0 \le j \le J \text{ and } (i = 0 \text{ or } i = I) \text{ for } 1 \le n \le \frac{N}{2} \\ \psi^n_{i,j} &= \beta \cdot \psi^{\frac{3N}{2}+1-n}_{0,j} \; ; 0 \le j \le J \text{ and } (i = 0 \text{ or } i = I) \text{ for } \frac{N}{2} \le n \le N \\ \psi^n_{i,j} &= \beta \cdot \psi^{N+1-n}_{0,j} \; ; 0 \le i \le I \text{ and } (j = 0 \text{ or } j = J) \text{ for } 1 \le n \le N \end{aligned} \tag{42}$$

such that $\Omega_n \cdot \vec{n} < 0$

$\beta = 0$ (vacuum condition) ; $\beta = 1$ (reflective condition) ; $\beta \in$ (0 , 1) (albedo condition)

The Periodic boundary condition can be defined by Eq. 43.

$$\begin{aligned} \psi^n_{0,j} &= \psi^n_{I,j} \qquad \text{with} \;\; 0 \le j \le J \qquad 1 \le n \le N \\ \psi^n_{i,0} &= \psi^n_{i,J} \qquad \text{with} \;\; 0 \le i \le I \qquad 1 \le n \le N \end{aligned} \tag{43}$$

2.4. Angular Quadratures

The discrete ordinates method S_n is commonly used in nuclear engineering to calculate a numerical solution of the integro-differential form of the Boltzmann transport equation. The method calculates the integral terms depending on the angles. Basically, the method consist in a numerical integration based on collocation points, which are the discrete directions and their weights. The combination of discrete angular directions and weights is called quadrature set.

Carlson and Lathrop proposed to use specialized quadrature sets [20, 21], that satisfy higher order moments of the direction cosines. For one dimensional cases, the scattering term only depends on one angular variable (polar angle or its direction cosine μ). This work analyzes the following Quadrature Sets for one-dimensional cases: Gauss-Legendre, Chebyshev type 1, and Chebyshev type 2. For two dimensional cases the following Quadrature Sets are studied: LQ_N (Level-Symmetric), $P_n - EW$ (Gauss-Legendre Equal Weight), $P_n - T_n$ (Gauss-Legendre Chebyshev) [22, 23, 24].

3. Numerical Results

The algorithms proposed in the previous section were implemented in a FORTRAN program called *n-DOTEC (neutron - Discrete Ordinates Transport Equation Code)*. This section shows *n-DOTEC* results for several one and two-dimensional problems or benchmarks. This section shows the results of eigenvalues and the neutron flux distribution or the power distribution. The results are evaluated by means of the eigenvalue errors, which are the relative errors multiplied by 10^5.

$$pcm = \frac{|ref.value - value|}{ref.value} \cdot 1 \times 10^5 \tag{44}$$

3.1. One-dimensional cases

To test the one-dimensional version of *n-DOTEC*, this section shows the results for several one-dimensional benchmark cases including different boundary conditions, both types of scattering (isotropic and anisotropic), different number of materials and different number of energy groups.

3.1.1. ISSA Benchmark

This is a one-energy one-dimensional slab problem with 2 regions, a fissile material on the left and a moderator material on the right (Fig.3). The material cross-sections are shown in Fig.3. The boundary condition on the left is reflective and on the right is vacuum. For the spatial discretization 100 mesh intervals were discretized. The Quadrature used was Gauss-Legendre and with an order of S_8. The four largest eigenvalues obtained with *n-DOTEC* were 1.67835, 0.798004, 0.451980, *and* 0.292597. The reference value of the largest eigenvalue (K_{eff}) is 1.67840 for S_{16} and 100 mesh intervals, calculated with ANISN (A One Dimensional Discrete Ordinates Transport Code With

Anisotropic Scattering) code supported by Oak Ridge National Laboratory [25]. The normalized scalar flux is displayed in Fig.4. As can be seen, the eigenvalue error is 2.979 *pcm*.

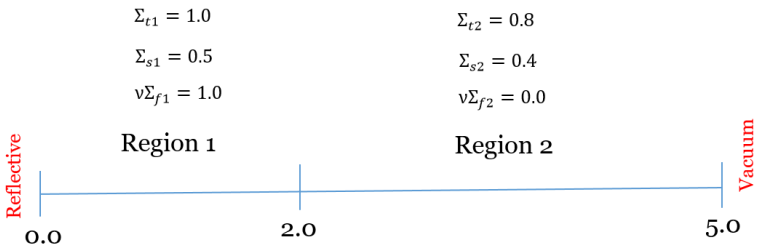

Figure 3: Geometry and cross sections for ISSA Benchmark

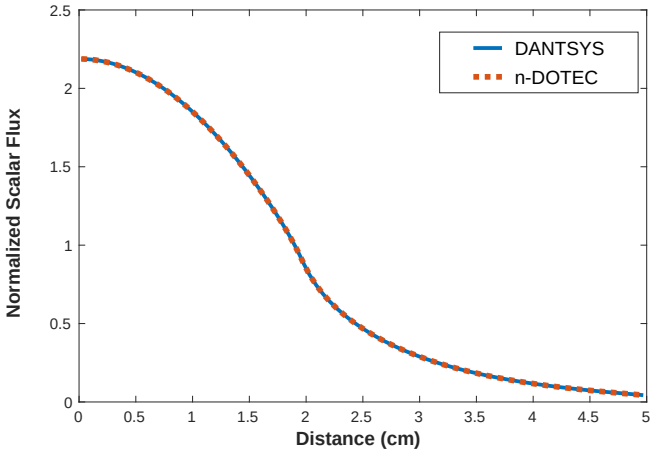

Figure 4: Normalized Scalar Flux for ISSA Benchmark calculated with $n - DOTEC$

3.1.2. Seven Alternate Region

This problem is composed of seven slab regions of three different combinations of fuel, reflector and absorber [26]. The one-energy group cross sections for these materials are shown in Table 1. Three different cases are considered, one without absorber, one with absorber in position 5 and another with absorber in position 6. A scheme is shown in Fig.5. All cases use vacuum conditions for both boundaries, on the left and right. Each region is subdivided into 50 fine mesh cells and Gauss-Legendre quadrature set was selected with an order of S_{32} for *n-DOTEC* simulation. Table 2 shows the results for the 3 largest eigenvalues. These results are compared with the reference values obtained by means of Green´s Function Method (GFM) [26]. Also, the first eigenvalue was

calculated by DANTSYS with 500 fine mesh cells in each region and S_{96}. One can see that the values obtained by *n-DOTEC* are in agreement with the reference values. The error eigenvalue error for the first eigenvalue in base case is 2.55 *pcm*, for the absorber in the position 5 is 141 *pcm* and for the absorber in the position 6 is 15 *pcm*. Figure 6 shows a comparison between *n-DOTEC* results and PARTISN results.

Table 1: Cross-Sections for Seven Region Slab

	$\nu\Sigma_f(cm^{-1})$	$\Sigma_s(cm^{-1})$	$\Sigma_t(cm^{-1})$
Fuel (U-235)	0.178	0.334	0.415
Reflector (Be)	0.0	0.334	0.371
Absorber (Be $w/c = 0.1$)	0.0	0.037	0.371

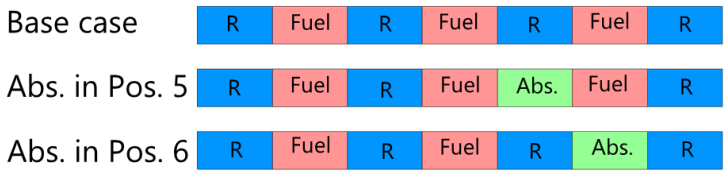

Figure 5: Cases for Seven Region Slab

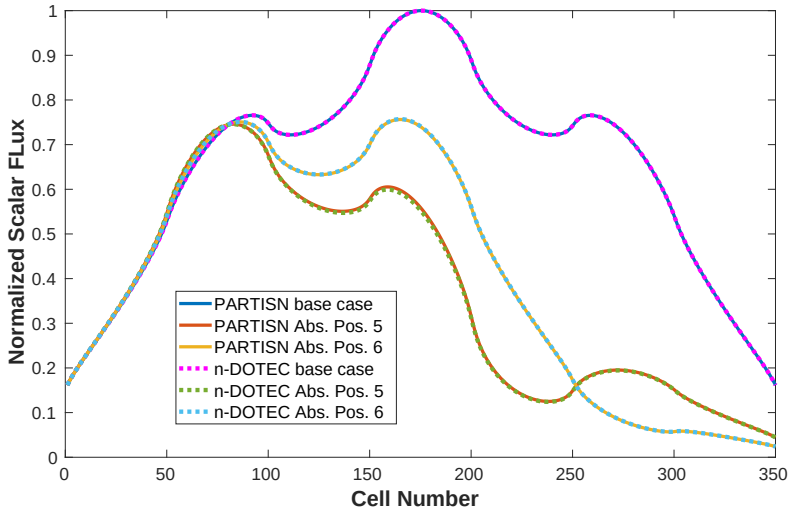

Figure 6: Scalar fluxes for each case of the 7 alternate region problem

Table 2: Seven-region eigenvalues

Case	nº Eigenvalue	GFM	DANTSYS	n-DOTEC	pcm (ΔK_{eff})
No absorber	1	1.17361	1.17361	1.17364	2.55
	2	0.758525	-	0.756857	219
	3	0.551768	-	0.549998	320
Abs. in Pos. 5	1	0.942676	-	0.941346	141
	2	0.655770	-	0.653801	300
	3	0.529032	-	0.527203	345
Abs. in Pos. 6	1	1.02265	1.02265	1.022493	15
	2	0.603382	-	0.601812	260
	3	0.208455	-	0.207234	585

3.1.3. Others

For the validation of the code, in addition to the aforementioned cases, several additional cases with isotropic and anisotropic scattering has been modeled according to the *Analytical Benchmark Test Set for Criticality Code Verification* [27]. Table 3 shows a resume of the results of the multiplication factor for different problems included in the analytical benchmark and the previous cases.

3.2. Two-dimensional cases

This section exhibits four more realistic cases used to test the two-dimensional version of *n-DOTEC* program. The first one is the *MOX test Problem*, which was selected to check vacumm boundary conditions and non-homogeneous systems. Next two cases test reflective conditions in an homogeneous fuel and non-homogeneous fuel with rods: *BWR cell test problem and BWR rod bundle test problem*. Finally, the last problem is the *C5G7 test problem*, a known 2-D fuel assembly benchmark on deterministic transport without spatial homogenization.

3.2.1. MOX test Problem

This problem is a modification of the MOX benchmark problem described in *Capilla et. al (2008)* [14] and adapted from *Brantley and Larsen (2000)* [28]. The core configuration is composed of 7×7 fuel assemblies of two types of fuel (MOX/UO_2) as can be seen in Fig.7. The core is surrounded by a reflector material and each assembly has dimensions of 21.42×21.42 cm. This problem has two-energy groups and three different materials. The cross sections are shown in Table 4. The boundary conditions are vacuum.

The order of discrete ordinates used by *n-DOTEC* was S_2 Gauss-Legendre Chebyshev ($P_n - T_n$) quadrature set, the spatial discretization was a mesh of 36×36 elements. The four dominant eigenvalues calculated by *n-DOTEC* were compared with those calculated with the Spherical Harmonics Nodal Collocation (SHNC) in *Capilla et. al (2008)* [14]. The comparison is shown in Table 5. In Figs.8 and 9, the scalar flux distribution is displayed for the second and

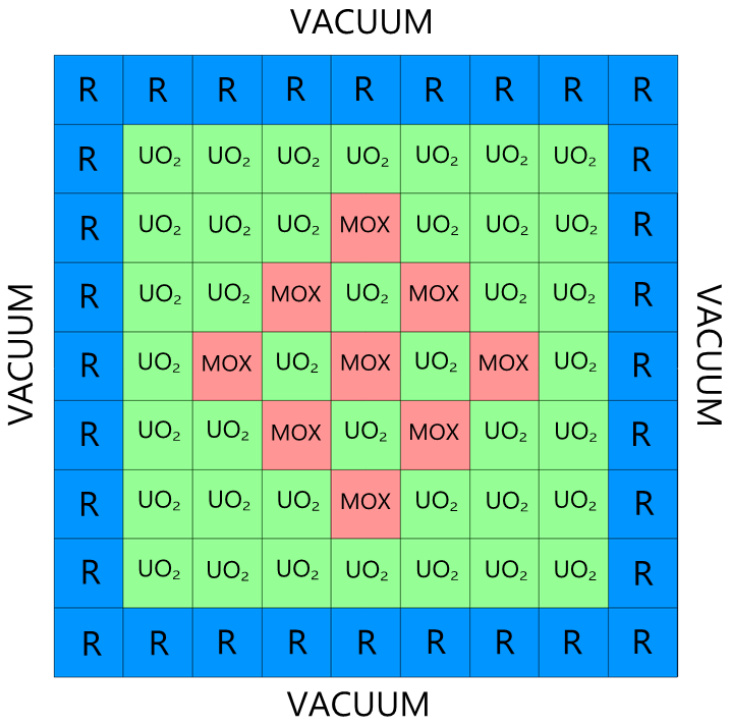

Figure 7: MOX benchmark problem geometry

third subcritical degenerated modes. The results show low errors for the first eigenmode, but these are slightly higher for the rest of eigenvalues.

3.2.2. BWR cell test problem

The second case is a homogeneous BWR cell [29, 30]. This case has been selected due to the fact that it considers upscattering. The problem is composed of a central homogenized fuel region surrounded by water moderator as can be seen in Fig. 10. The two energy group cross-sections are shown for the two materials of the problem in Table 6. All boundary conditions are reflective. The number of mesh intervals considered are 30×30 and the quadrature set used for different orders is $P_n - T_n$. The four largest eigenvalues were calulated, but only the first eigenmode was compared. The reference infinity multiplication factor calculated with SURCU code developed at Federal Institute of Technology, Zurich, Switzerland (that uses Quadruple Spherical Harmonics) is 1.2127 as can be seen in *J. Stepanek et al.* [29]. In addition, results from DANTSYS were also compared. Table 7 shows *n-DOTEC* results for different orders of the quadrature sets. Only the first group flux distribution for the four dominant eigenvalues can be seen in Fig. 11. The second energy group is not showed due to the extent of the paper. The K_{eff} calculated with S_8 has an error of 20 *pcm* with respect to the reference and 0.083 *pcm* with respect to DANTSYS with

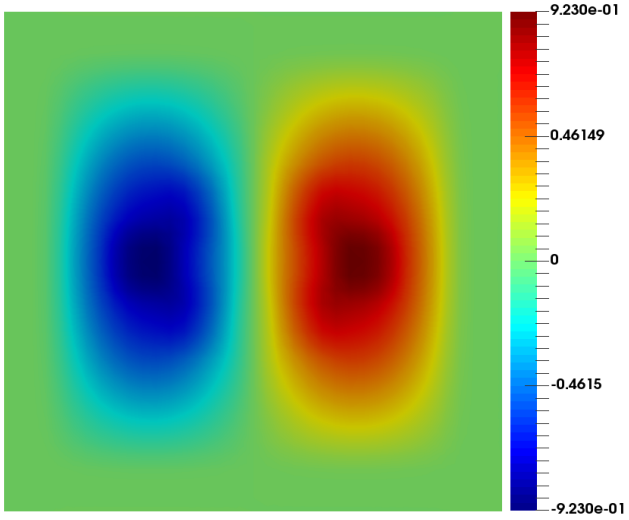

Figure 8: Scalar flux distribution for 2nd eigenvalue

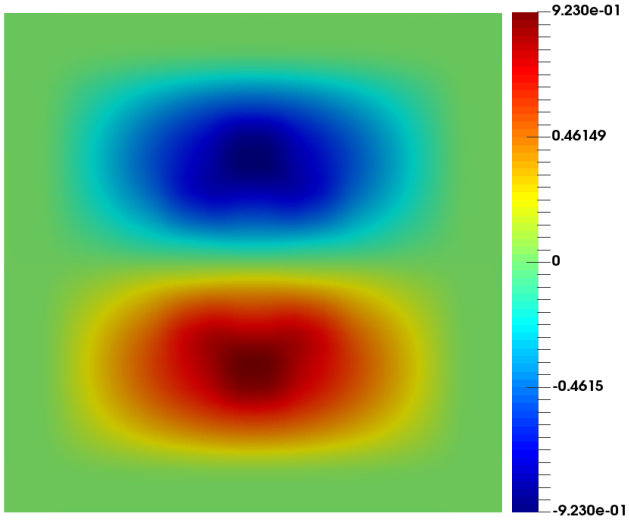

Figure 9: Scalar flux distribution for 3rd eigenvalue

the same quadrature set and order.

3.2.3. BWR rod bundle test problem

This test problem is a two-dimensional fuel bundle of BWR [30, 31]. There are seven materials in this case: materials ranging from 1 to 4 are different fuel

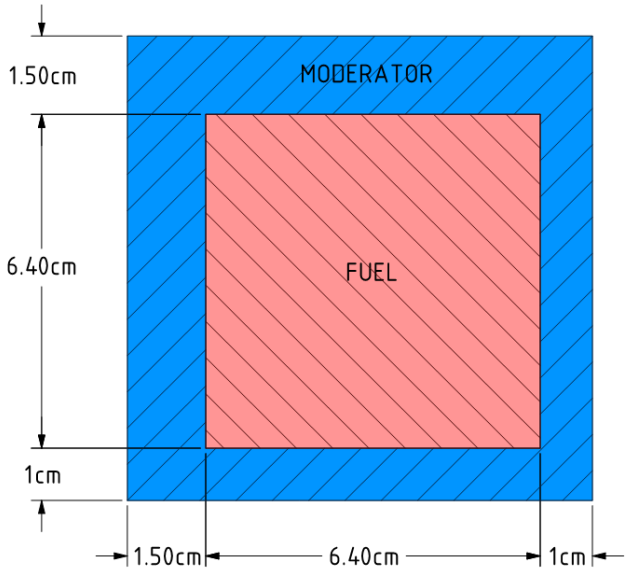

Figure 10: BWR cell problem geometry.

types, material 5 is an homogenized fuel with poison. Surrounding these materials there is a wall assembly of stainless steel (material 6) which is surrounded by water (material 7). A scheme of this geometry configuration is shown in Fig. 12. The problem has two energy groups and the cross-sections are displayed in Table 8. All boundary conditions are reflective. The *n-DOTEC* simulation used a spatial discretization of 1×1 for each cell of the problem and different Legendre-Chebyshev ($P_n - T_n$) quadrature orders. The reference solution for this problem was calculated by using a mesh of 4×4 and angular approximation S_8 by DOT code. Table 9 shows a comparison of the results. The eigenvalue error with respect to the reference is 49 *pcm* for S_8 order and 7 *pcm* with respect to DANTSYS.

3.2.4. C5G7 test problem

This case corresponds to a quarter symmetric core of the PWR C5G7 MOX fuel assembly problem [32]. The benchmark geometry is composed of 4 assemblies surrounded by a water reflector region, as can be seen in Fig. 14. as well as the boundary conditions. Each fuel assembly is made up of 17×17 square pitch array of cylindrical fuel pins. Since *n-DOTEC* can only deal with Cartesian geometry, this cylindrical pin is modeled by a square with the same area as the corresponding cylinder. A representation of this approximation is displayed in Fig. 15. The composition layout and the mesh is shown Fig. 16. In addition, in Fig. 17 displays a zoomed detail of Fig. 16. Cross-sections are described in the benchmark [32], with 7 energy groups for the seven corre-

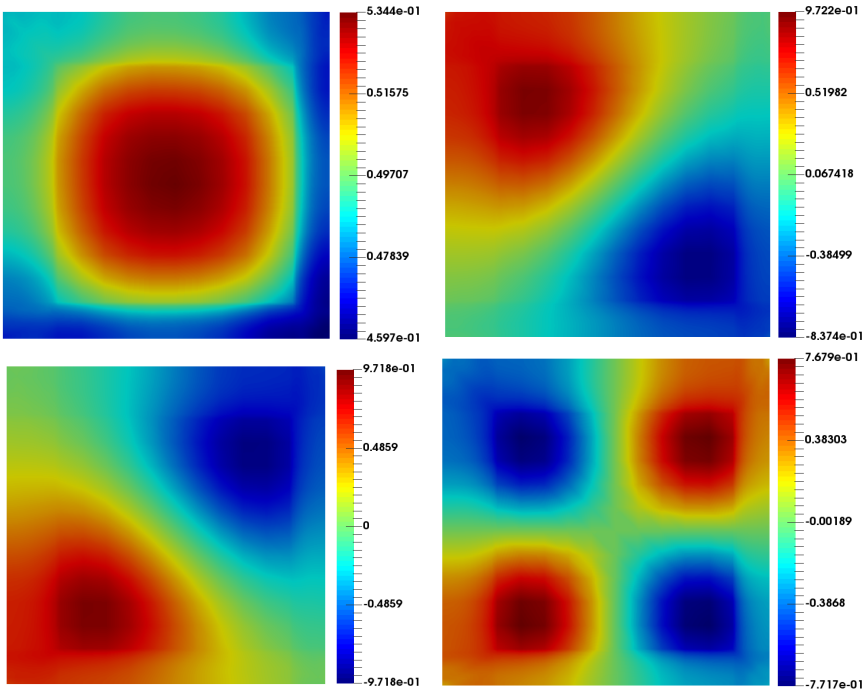

Figure 11: Four dominant eigenvalues flux distribution for the BWR cell test problem.

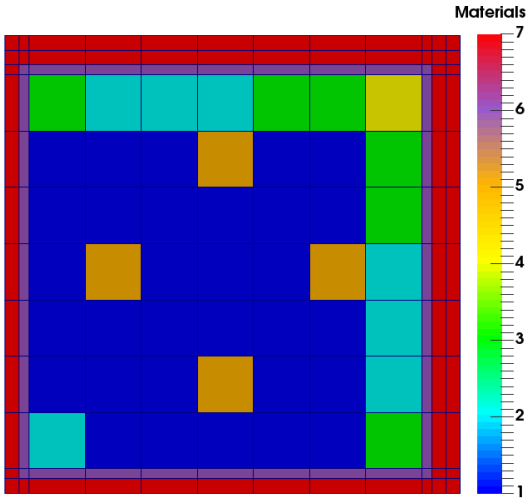

Figure 12: Material distribution and mesh for the BWR rod bundle test problem.

315 sponding materials. The reactor is composed of three MOX fuels with different enrichments, UO_2 fuels, guide tubes, fission chambers and moderator. Table

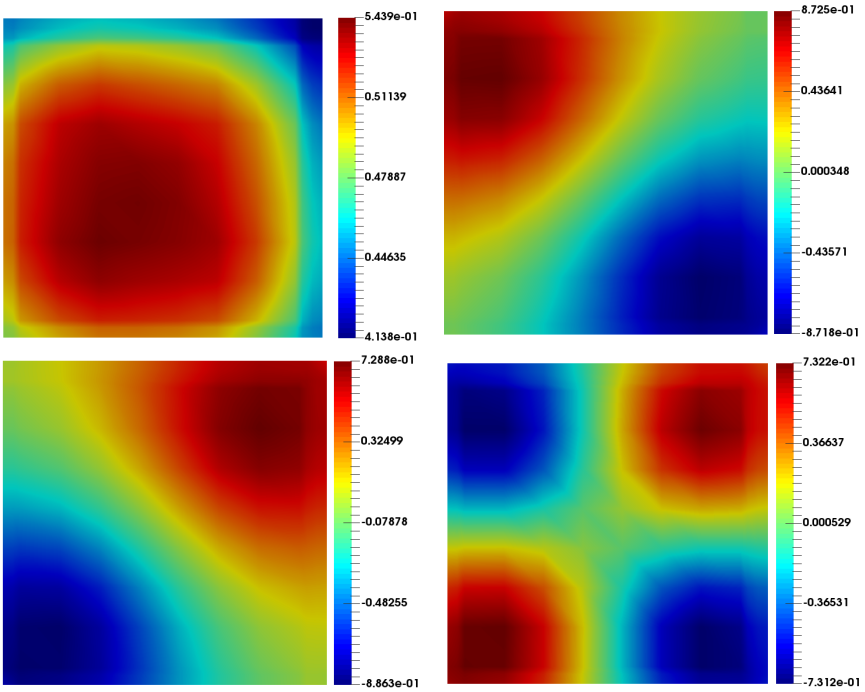

Figure 13: Four dominant eigenvalues flux distribution for the BWR rod bundle test problem.

11 resumes the comparison of results obtained by *n-DOTEC* with $S4$ and $S8$ $P_n - T_n$ quadrature and those obtained by MCNP, which is the reference code. The K_{eff} error is 88 *pcm* for S_4 order and the mean relative error is 1.413 %. Other power comparison results show good agreement with respect to the benchmark results. Furthermore, the sub-critical modes have been compared in the 10, where it can be seen that the result is independent of the any kind of angular discretization [33].

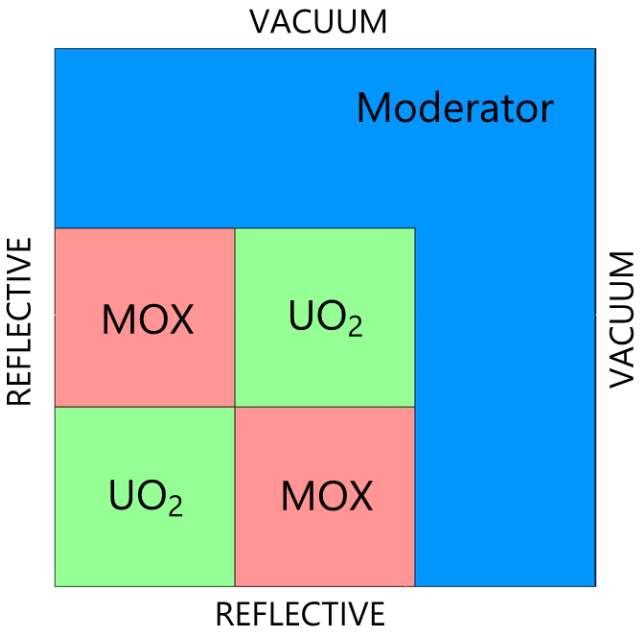

Figure 14: Assembly.

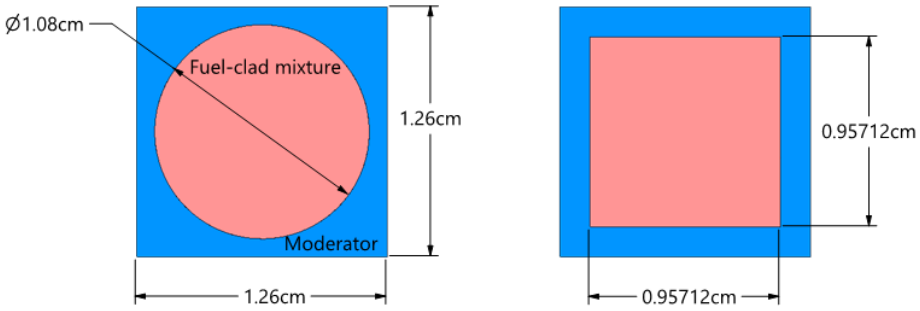

Figure 15: Pin cell approximation.

Table 3: Analytical Benchmark Results. **AB=Analytical Benchmarck* [27].

Scattering	Groups	Reference	Problem Description	Ref. Value	n-DOTEC	pcm (ΔK_{eff})
ISOTROPIC	ONE-ENERGY GROUP	ISSA Benchmark	2 Regions, reflective condition on the left and vacuum on the right	1.67840	1.67835	3.28
		7 alternate regions	Base case	1.17361	1.17364	2.47
		AB* (Problem 3)	Non Symmetric Slab with H_2O Reflector	1.00000	0.99987	12.9
		AB* (Problem 4)	Symmetric Slab with H_2O Reflector	1.00000	0.99991	9.2
	TWO-ENERGY GROUP	AB* (Problem 45)	One Medium Slab Pu^{239}	1.00000	0.99987	13.4
		AB* (Problem 48)	One Medium Slab U^{235}	1.00000	0.99993	7.5
		AB* (Problem 58)	Two-media slab $U^{235}+H_2O$	1.00000	0.99998	1.9
	THREE-ENERGY GROUP	AB* (Problem 74)	One medium infinite slab	1.60000	1.60000	0
	SIX-ENERGY GROUP	AB* (Problem 75)	One medium infinite slab	1.60000	1.60000	0
ANISOTROPIC	TWO-ENERGY GROUP	AB* (Problem 70)	One medium infinite slab	1.63145	1.63145	0.12
		AB* (Problem 71)	One medium finite slab	1.00000	0.99998	2.5

Table 4: MOX benchmark problem cross-sections. g=1 (fast energy group), g=2 (thermal energy group).

Material	Group	Σ_t	$\nu\Sigma_f$	$\Sigma_{s,1\to g}$	$\Sigma_{s,2\to g}$	χ_g
MOX fuel	1	0.550	0.0075	0.520	-	1.000
	2	1.060	0.450	0.015	0.760	0.000
UO_2 fuel	1	0.570	0.005	0.540	-	1.000
	2	1.100	0.125	0.020	1.000	0.000
Reflector	1	0.611	0.000	0.560	-	0.000
	2	2.340	0.000	0.050	2.300	0.000

Table 5: Dominant eigenvalues for the MOX problem. **SHNC=Spherical Harmonics Nodal Collocation.*

Eigenvalue	SHNC*	*n-DOTEC* Leg-Cheby S_2	pcm (ΔK_{eff})
K_{eff}	0.9925	0.992538	3
2nd eigen.	0.9665	0.966344	16
3rd eigen.	0.9665	0.966344	16
4th eigen.	0.9399	0.939566	35

Table 6: BWR cell benchmark problem cross-sections. g=1 (fast energy group), g=2 (thermal energy group).

Material	Group	Σ_t	$\nu\Sigma_f$	$\Sigma_{s,1\to g}$	$\Sigma_{s,2\to g}$	χ_g
Fuel	1	0.196647	0.006203	0.178000	0.001089	1.000
	2	0.596159	0.1101	0.010020	0.525500	0.000
Moderator	1	0.222064	0.000	0.199500	0.001558	0.000
	2	0.887874	0.000	0.021880	0.878300	0.000

Table 7: BWR cell benchmark problem multiplication factor results for different quadrature order.

	Order	Quadrature	nº of angular directions	K_{eff}	pcm (ΔK_{eff})
Reference value	-	-	-	1.2127	-
n-DOTEC	S_2	Leg-Cheby	4	1.218693	494
DANTSYS	S_2	Leg-Cheby	4	1.21869384	494
n-DOTEC	S_4	Leg-Cheby	12	1.214271	129
DANTSYS	S_4	Leg-Cheby	12	1.21427157	129
n-DOTEC	S_8	Leg-Cheby	40	1.212944	20
DANTSYS	S_8	Leg-Cheby	40	1.21294501	20

Table 8: BWR rod bundle benchmark problem cross-sections. g=1 (fast energy group), g=2 (thermal energy group).

Material	Group	Σ_t	$\nu\Sigma_f$	$\Sigma_{s,1\to g}$	$\Sigma_{s,2\to g}$	χ_g
1	1	0.253100	0.0059250	0.2334270	-	1.000
	2	0.573200	0.0981700	0.010690	0.514280	0.000
2	1	0.253600	0.0052420	0.2339200	-	1.000
	2	0.576700	0.0822800	0.010950	0.524960	0.000
3	1	0.253500	0.0048200	0.2337900	-	1.000
	2	0.579070	0.0720000	0.011120	0.532530	0.000
4	1	0.253300	0.0043370	0.2336900	-	1.000
	2	0.583700	0.0590000	0.011130	0.542300	0.000
5	1	0.250600	0.0056050	0.2308400	-	1.000
	2	0.585300	0.0242400	0.010160	0.422700	0.000
6	1	0.217200	0.0000000	0.2070700	-	0.000
	2	0.474800	0.0000000	0.009095	0.470416	0.000
7	1	0.247600	0.0000000	0.2105800	-	0.000
	2	1.123000	0.0000000	0.036820	1.115200	0.000

Table 9: BWR rod bundle benchmark problem multiplication factor results for different quadrature order.

	Order	Quadrature	nº of angular directions	K_{eff}	pcm (ΔK_{eff})
Reference DOT	S_8	-	40	1.08714	-
n-DOTEC	S_2	Leg-Cheby	4	1.092126	458
DANTSYS	S_2	Leg-Cheby	4	1.09245586	488
n-DOTEC	S_4	Leg-Cheby	12	1.088717	145
DANTSYS	S_4	Leg-Cheby	12	1.08881782	154
n-DOTEC	S_8	Leg-Cheby	40	1.087596	41
DANTSYS	S_8	Leg-Cheby	40	1.08768147	49

Table 10: Sub-critical modes comparison. [1] *SHNC=Spherical Harmonics Nodal Collocation.*

mode	*n-DOTEC S2*	*n-DOTEC S4*	[1]SHNC P1	[1]SHNC P3
1st	1.188877	1.187619	1.183847	1.177241
2nd	0.912220	0.918477	0.904490	0.910234
3rd	0.868536	0.873095	0.859548	0.867538
4th	0.730518	0.727383	0.703131	0.719696
5th	0.571266	0.592365	0.562243	0.587400
6th	0.570752	0.591601	0.561512	0.586667

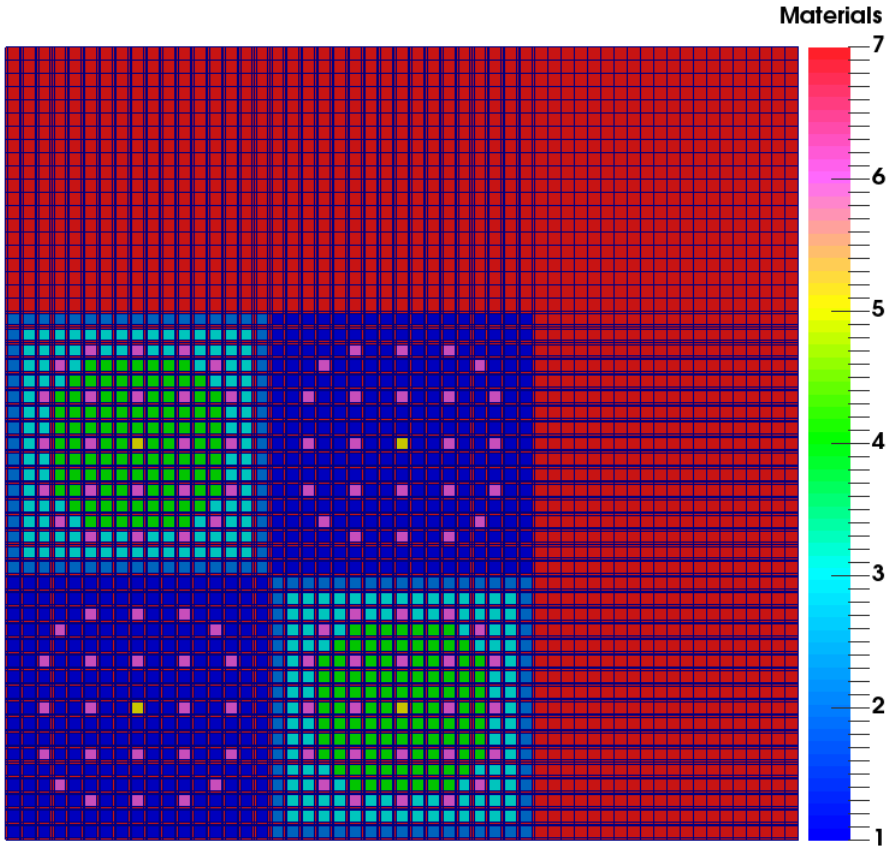

Figure 16: composition layout.

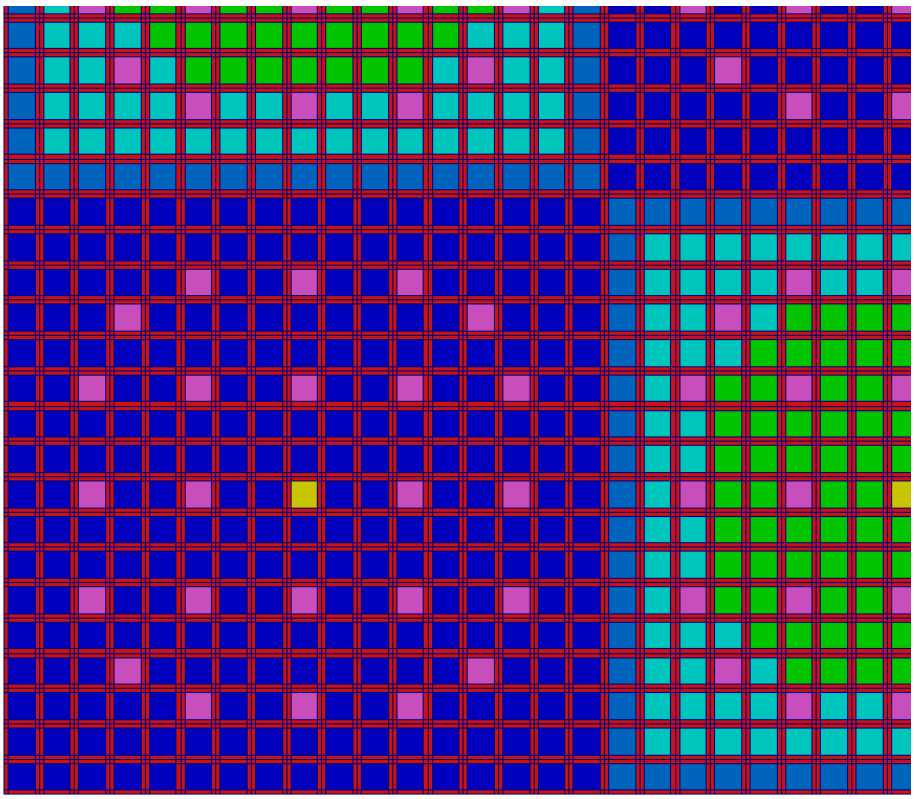

Figure 17: composition layout.

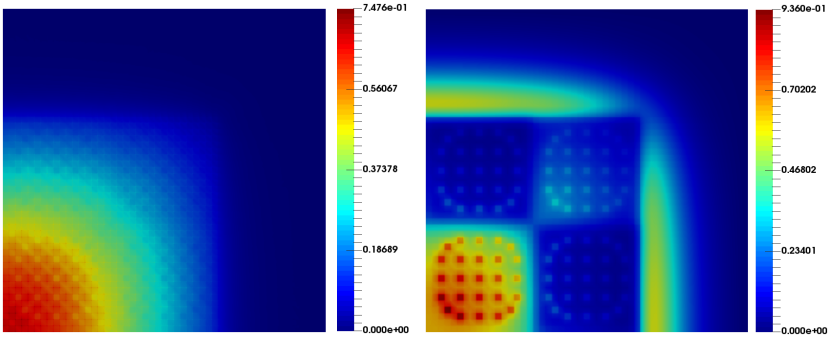

Figure 18: Flux 1st eugenvalue for energy groups 1 and 7.

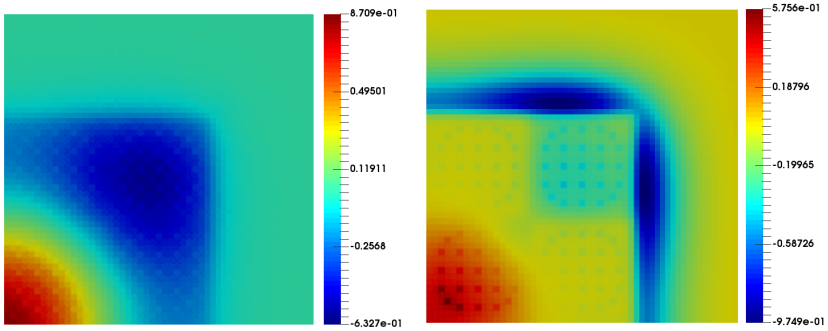

Figure 19: Flux 2nd eigenvalue for energy groups 1 and 7.

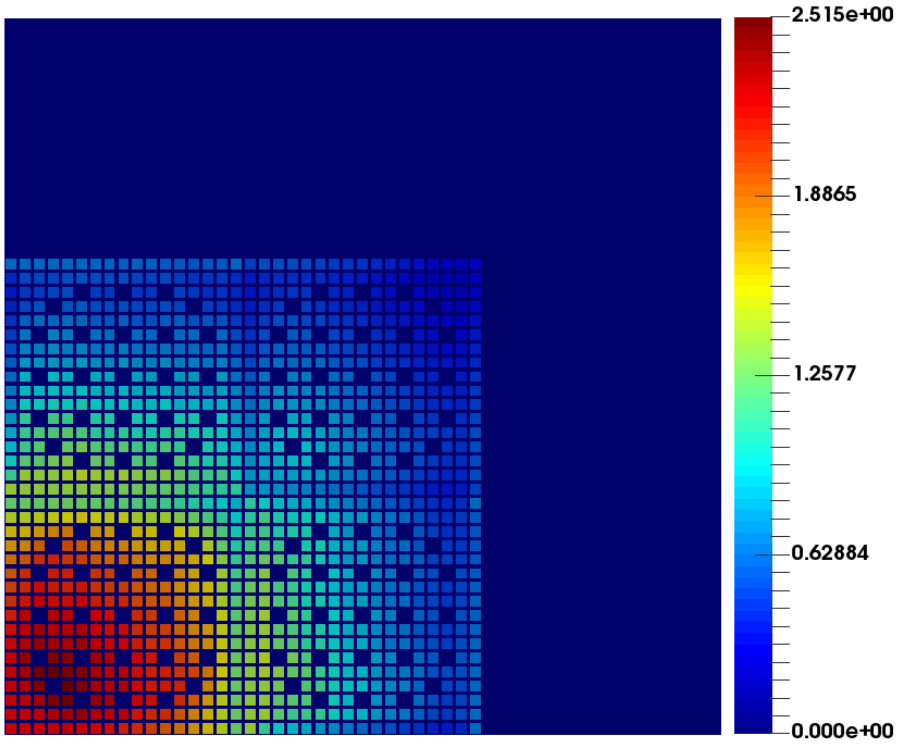

Figure 20: Power Distribution of C5G7 problem.

Table 11: C5G7 Test problem results.

	Quad.	n° dir	K_{eff}	pcm	Max. Perc. Error	Average Error	Mean Rel. Error	Avg.Pin Power	Max.Pin Power	Min.Pin Power	UO_2-1 Avg.Pin Power	MOX Avg.Pin Power	UO_2-2 Avg.Pin Power
MCNP Ref.	-	-	1.18655	-	-	-	-	1.000	2.498	0.232	1.867	0.802	0.529
n-DOTEC	Leg-Cheby	4	1.1888	190	10.785	3.762	3.352	1.000	2.520	0.227	1.840	0.824	0.513
n-DOTEC	Leg-Cheby	12	1.1876	88	6.745	2.110	1.802	1.000	2.515	0.223	1.852	0.817	0.514

4. Conclusions

The method explained in this work solves the one and two-dimensional steady-state multi-group neutron transport equation using Cartesian geometry. Spatial and angular discretization were performed with Finite Difference Method and Discrete Ordinates Method, respectively. The method is capable of calculating multiple eigenvalues with a simple formulation. The method can consider both kind of scattering: isotropic and anisotropic. The algorithms have been programmed in a FORTRAN code called *n-DOTEC*. This program has been validated with several one-dimensional benchmarks and four two-dimensional benchmarks. The four realistic two-dimensional problems selected are *MOX test problem*, *BWR cell test problem*, *BWR rod bundle test problem* and *C5G7 test problem*. The methodology used in this work shows that *n-DOTEC 1D* results show good agreement with reference values, even when anisotropic scattering is considered. Moreover, *n-DOTEC 2D* is capable of modeling cylindrical geometries without spatial homogenization under the simplification of Cartesian. This modeling was tested in the C5G7 benchmark, which obtains good results and it demonstrates that the code is capable of simulating any number of energy groups. Because the calculation time increases with the spatial or angular discretization and with the number of groups, for practical purposes in the future it is expected to implement the algorithms in parallel to accelerate the calculations.In addition, future works will develop the solution for nonmultiplying systems with other kind of particles (photons) and the solution of problems with fixed source, which are interesting in shielding and radiation protection.

Acknowledgments

This work has been partially supported by the Spanish Agencia Estatal de Investigación [grant number BES-2016-076782], Ministerio de Eduación Cultura y Deporte [grant number FPU13/01009] and the Spanish Ministerio de Economia Industria y Competitividad [project ENE2015-68353-P].

References

[1] D. G. Cacuci, Handbook of Nuclear Engineering: Vol. 1: Nuclear Engineering Fundamentals; Vol. 2: Reactor Design; Vol. 3: Reactor Analysis; Vol. 4: Reactors of Generations III and IV; Vol. 5: Fuel Cycles, Decommissioning, Waste Disposal and Safeguards, Vol. 2, Springer Science & Business Media, 2010.

[2] K. D. Lathrop, Ray effects in discrete ordinates equations, Nuclear Science and Engineering 32 (3) (1968) 357–369.

[3] A. Hébert, Applied reactor physics, Presses inter Polytechnique, 2009.

[4] Y. Azmy, E. Sartori, Nuclear computational science: a century in review, Springer, 2010.

[5] V. Hernandez, J. E. Roman, V. Vidal, Slepc: A scalable and flexible toolkit for the solution of eigenvalue problems, ACM Transactions on Mathematical Software (TOMS) 31 (3) (2005) 351–362.

[6] S. Balay, S. Abhyankar, M. F. Adams, J. Brown, P. Brune, K. Buschelman, L. Dalcin, A. Dener, V. Eijkhout, W. D. Gropp, D. Karpeyev, D. Kaushik, M. G. Knepley, D. A. May, L. C. McInnes, R. T. Mills, T. Munson, K. Rupp, P. Sanan, B. F. Smith, S. Zampini, H. Zhang, H. Zhang, PETSc users manual, Tech. Rep. ANL-95/11 - Revision 3.11, Argonne National Laboratory (2019).
URL `http://www.mcs.anl.gov/petsc`

[7] W. Rhoades, R. Childs, Dort/tort two-and three-dimensional discrete ordinates transport, version 2.7. 3. ornl, oak ridge, Tech. rep., RSIC-CCC-543 (1993).

[8] R. E. Alcouffe, R. S. Baker, F. W. Brinkley, D. R. Marr, R. D. O'Dell, W. F. Walters, Dantsys: a diffusion accelerated neutral particle transport code system.

[9] R. E. Alcouffe, R. S. Baker, J. A. Dahl, S. A. Turner, R. Ward, Partisn: A time-dependent, parallel neutral particle transport code system, Los Alamos National Laboratory, LA-UR-05-3925 (May 2005).

[10] G. Sjoden, A. Haghighat, Pentran™: Parallel environment neutral particle transport in 3-d cartesian geometry, in: Proc. Int. Conf. on Mathematical Methods and Supercomputing for Nuclear Applications, 1997, pp. 232–234.

[11] G. Marleau, A. Hébert, R. Roy, A user guide for dragon 3.06, Report IGE-174 Rev 7.

[12] B. Collins, B. Kochunas, T. Downar, Assessment of the 2d moc solver in mpact: Michigan parallel characteristics transport code, in: Proceedings of the 2013 International Conference on Mathematics and Computational Methods Applied to Nuclear Science and Engineering-M and C 2013, 2013.

[13] Y. Jung, ntracer v1. 0 methodology manual, SNURPL-CM001 (10), Seoul National University Reactor Physics Laboratory, Seoul, Republic of Korea.

[14] M. Capilla, C. Talavera, D. Ginestar, G. Verdú, A nodal collocation approximation for the multi-dimensional pl equations–2d applications, Annals of Nuclear Energy 35 (10) (2008) 1820–1830.

[15] R. Koch, R. Becker, Evaluation of quadrature schemes for the discrete ordinates method, Journal of Quantitative Spectroscopy and Radiative Transfer 84 (4) (2004) 423–435.

[16] I. Abu-Shumays, Angular quadratures for improved transport computations, Transport Theory and Statistical Physics 30 (2-3) (2001) 169–204.

[17] E. E. Lewis, W. F. Miller Jr, Computational methods of neutron transport. 1984.

[18] G. Bell, S. Glasstone, Nuclear reactor theory, krieger (1985).

[19] Á. Bernal García, Development of a 3d modal neutron code with the finite volume method for the diffusion and discrete ordinates transport equations. application to nuclear safety analyses, Ph.D. thesis (2018).

[20] K. D. Lathrop, B. G. Carlson, Discrete ordinates angular quadrature of the neutron transport equation, Tech. rep., Los Alamos Scientific Lab., N. Mex. (1964).

[21] B. G. Carlson, Tables of equal weight quadrature eqn over the unit sphere, Los Alamos Scientific Laboratory of the University of California, 1971.

[22] B. G. Carlson, Transport theory: Discrete ordinates quadrature over the unit sphere., Tech. rep., Los Alamos Scientific Lab., N. Mex. (1970).

[23] S. D. Wai, D. Gottlieb, The chebyshev-legendre method: Implementing legendre methods on chebyshev points, Tech. rep., INSTITUTE FOR COMPUTER APPLICATIONS IN SCIENCE AND ENGINEERING HAMPTON VA (1993).

[24] W. F. Walters, Use of the chebyshev-legendre quadrature set in discrete-ordinate codes, Tech. rep., Los Alamos National Lab., NM (USA) (1987).

[25] J. Issa, N. Riyait, A. Goddard, G. Stott, Multigroup application of the anisotropic fem code feltran to one, two, three-dimensions and rz problems, Progress in Nuclear Energy 18 (1-2) (1986) 251–264.

[26] D. E. Kornreich, D. K. Parsons, The green's function method for effective multiplication benchmark calculations in multi-region slab geometry, Annals of Nuclear Energy 31 (13) (2004) 1477–1494.

[27] A. Sood, R. A. Forster, D. K. Parsons, Analytical benchmark test set for criticality code verification, Progress in Nuclear Energy 42 (1) (2003) 55–106.

[28] P. S. Brantley, E. W. Larsen, The simplified p 3 approximation, Nuclear Science and Engineering 134 (1) (2000) 1–21.

[29] J. Stepanek, T. Auerbach, W. Hälg, Calculation of four thermal reactor benchmark problems in xy geometry, Tech. rep., Eidgenoessisches Inst. fuer Reaktorforschung (1982).

[30] S. Kashi, A. Minuchehr, A. Zolfaghari, B. Rokrok, Mesh-free method for numerical solution of the multi-group discrete ordinate neutron transport equation, Annals of Nuclear Energy 106 (2017) 51–63.

[31] B. Zolotar, F. Rahn, Bwr rod bundle benchmark problem, Transactions of the American Nuclear Society 23.

[32] M. Smith, E. Lewis, B. Na, Benchmark on deterministic transport calculations without spatial homogenization: A 2-d/3-d mox fuel assembly 3-d benchmark (2003).

[33] M. Capilla, C. Talavera, D. Ginestar, G. Verdú, Numerical analysis of the 2d c5g7 mox benchmark using pl equations and a nodal collocation method, Annals of Nuclear Energy 114 (2018) 32–41.